Simple construction of Rydberg quantum cloning machines via nonadiabatic geometric quantum operations

X.-Y. Zhu,[1,2] B.-L. Fang,[3,4,*] Y.-H. Li,[1] F.-Q. Guo,[1] E.-J. Liang,[1,†] L.-L. Yan,[1,‡] and S.-L. Su[1,§]

[1]*School of Physics and Microelectronics, Key Laboratory of Materials Physics of Ministry of Education, Zhengzhou University, Zhengzhou 450001, China*

[2]*College of Science, Henan University of Engineering, Zhengzhou 451191, China*

[3]*Department of Physics, School of Advanced Manufacturing Engineering, Hefei University, Hefei, Anhui 230022, People's Republic of China*

[4]*Hefei Institute of Environmental Engineering, Hefei University, Hefei, Anhui 230022, People's Republic of China*

(Received 14 July 2022; revised 8 September 2022; accepted 31 October 2022; published 17 November 2022)

A theoretical scheme based on the nonadiabatic geometric quantum computation (NGQC) is proposed to realize quantum cloning in the Rydberg atom system. In contrast to previous schemes, the present one utilizes the NGQC to construct the clone machine and thus is more robust against control errors. Meanwhile, to implement the desired cloning framework in the quantum clone machine, the scheme reported by Zhu and Ye [M.-Z. Zhu and L. Ye, Phys. Rev. A **91**, 042319 (2015)] based on cavity QED requires a series of single(two)-qubit operations. For the present NGQC-based scheme, through modulating the rotation angle of geometric operations, we can greatly simplify the process of realizing the cloning framework. In addition, through adjusting the relevant parameters, the scheme can perform symmetrical (asymmetrical) universal cloning, optimal symmetrical (asymmetrical) phase-covariant quantum cloning, and optimal symmetrical (asymmetrical) real-state quantum cloning. The present attempt to optimize quantum cloning using geometric quantum control in Rydberg atoms provides a path to robust and simplified quantum cloning, which is meaningful for experiments and has implications for quantum cloning in other quantum systems as well.

DOI: 10.1103/PhysRevA.106.052419

I. INTRODUCTION

As restricted by the no-cloning theorem developed by Wootters and Zurek [1], under the limitation of the linearity and superposition of quantum mechanics, the ideal replication of arbitrary unknown quantum states is impossible. Despite the fact that a perfect copy cannot be reached, approximate quantum cloning has attracted extensive attention since the optimal symmetrical universal quantum cloning machine (UQCM), which clones the arbitrary input states whose amplitude and phase are both unknown was proposed by Bužek and Hillery [2] and the optimality was proved in Refs. [3–5]. In 2011, Wang *et al*. proposed a unified way to realize a UQCM [6] in which the cloning procession uses symmetrical projection and this would reduce the difficulty of implementation. Compared with the UQCM, the phase-covariant cloning machine (PCCM) [7–16], which clones the input states with the amplitude is known and the phase is unknown and the real-state cloning machine (RSCM) [13,17,18] with the phase is known and the amplitude is unknown, can provide higher fidelities. The investigation of quantum cloning provides insight into other fundamental theories of quantum mechanics, e.g., the no-signal theorem [19,20] and no-broadcasting theorem [21,22]. Additionally, we can use quantum cloning to practically attack the quantum key distribution (QKD) protocol or analyze the security of the QKD protocol [23–27]. According to the symmetry, there are two types of approximate quantum cloning machines: symmetrical quantum cloning machines [28] and asymmetrical quantum cloning machines [17,29–34]. Recently, due to its theoretical and practical value, quantum cloning has attracted numerous theoretical and experimental endeavors in various physical systems [35–39]. In Ref. [18], different types of quantum cloning machines were implemented by employing the interaction between electron-spin and optical coherent pulse. They have the advantage that the coefficients of the three-qubit entangled state for the cloning machine framework are only the products of two trigonometric functions, so the cloning machine with different types can be readily implemented by adjusting the related parameters. However, the cloning framework needs to be prepared by one U_{23} operation and three controlled-NOT (CNOT) operations in which the implementation of the U_{23} operation and the CNOT operations requires a series of single(two)-qubit operations, which may increase the impact of decoherence.

The Rydberg atom possesses a long-lived highly excited state and long-range interaction, which makes it a particularly attractive physical platform for quantum information processing [40]. Within the blockade radius, when atoms are exited to high Rydberg states, only one atom can be excited at most, which is called the Rydberg blockade. This effect was widely studied theoretically and observed experimentally [41,42]. The pioneering work of the fast quantum gate operation based on the Rydberg blockade mechanism was proposed by Jaksch *et al*. [43]; after that many other applications were also proposed, such as

*fbl@hfuu.edu.cn
†ejliang@zzu.edu.cn
‡llyan@zzu.edu.cn
§To whom correspondence should be addressed: slsu@zzu.edu.cn

quantum entangled state preparation [44–47], quantum computation [48–51], quantum algorithms [52–54], and quantum simulators [55–58]. However, the realization of the quantum cloning in Rydberg atoms has not been well studied.

With the continuous development of quantum computation, nonadiabatic geometric quantum computation (NGQC) [59,60] based on the non-Abelian phase has attracted extensive attention due to its advantages of a robust geometric phase for some parameter fluctuations and having no need to meet adiabatic conditions. Since then, various theoretical and experimental schemes of NGQC based on non-Abelian theory were proposed [61–65], such as single-loop [66,67], single-shot-shaped [61,68–71], and dynamic decoupling [62,72]. Here we use the optimized NGQC implemented in general cases [61] to ensure flexibility and fault tolerance. Since the first nonadiabatic geometric quantum computation scheme based on the Rydberg atom proposed in Ref. [73], geometric gates have been realized based on different methods in the Rydberg atom. For instance, in Ref. [74], an implementation scheme of single- and two-qubit geometric gates via the nonadiabatic noncyclic non-Abelian geometric phase was proposed. In Ref. [75], a scheme to realize a three-qubit controlled gate based on the time-optimized nonadiabatic holonomic method in one step in the Rydberg atom was proposed. These schemes all provided ideas for implementing geometric quantum computation in Rydberg atoms.

In this paper, based on the optimized NGQC in the Rydberg atom system, we implement geometric gates that eliminate the accumulation of dynamic phases as a whole, which ensures the flexibility of the scheme, and on this basis, we propose a scheme to realize $1 \rightarrow 2$ optimal symmetric (asymmetric) UQCM [2,30,34], optimal symmetric (asymmetric) PCCM [14,15], optimal symmetric (asymmetric) RSCM [7,17], and optimal $1 \rightarrow 3$ symmetric economical RSCM (SERSCM) [9] with Rydberg atoms in which "$1 \rightarrow 2$" means one input qubit and two copied output qubits, "$1 \rightarrow 3$" means one input qubit and three copied output qubits, and "economical" means no auxiliary state is required. Based on the optimized NGQC scheme, the U_{23} and the CNOT operations required to implement the quantum cloning framework [18] are realized directly, respectively, which not only enhances the robustness of the scheme to control errors and decoherence, but also greatly simplifies the operational steps of the quantum cloning scheme and offers the possibility of experimental implementation.

The structure of the paper is as follows. In Sec. II, we propose to realize the optimized single- and two-qubit NGQC gates in Rydberg atoms. In Sec. III, we show how to implement different types of quantum cloning machines based on the proposed gates and plot the the analytical values of the fidelities for $1 \rightarrow 2$ asymmetric UQCM and PCCM. In Sec. IV, we discuss the dissipation effects caused by the spontaneous emission of atoms and the influence of environment-induced quasistatic noise on fidelity.

II. RYDBERG GEOMETRIC QUANTUM GATES

A. Arbitrary single-qubit geometric gate based on Rydberg atom

We consider a single Rydberg atom which consists of two hyperfine-Zeeman ground states $|0\rangle$, $|1\rangle$, and a Rydberg state $|r\rangle$. We use the resonance control field with Rabi frequency $\Omega_0(t)e^{i\varphi_0}$ [$\Omega_1(t)e^{i\varphi_1}$] to drive the transition $|0\rangle \rightarrow |r\rangle$($|1\rangle \rightarrow |r\rangle$) in which φ_0 and φ_1 are time-independent phases. The following Hamiltonian of the single Rydberg atom coupled by an external laser field in the interaction picture can be obtained by the rotating-wave approximation ($\hbar = 1$):

$$H = \frac{1}{2}[\Omega_0(t)|0\rangle\langle r|e^{i\varphi_0} + \Omega_1(t)|1\rangle\langle r|e^{i\varphi_1}] + \text{H.c.} \quad (1)$$

To realize the nonadiabatic geometric gate, we set $\Omega = \sqrt{\Omega_0^2 + \Omega_1^2}$, $\tan(\xi/2) = -\Omega_0/\Omega_1$, and $\varphi = \varphi_0 - \varphi_1$ with ξ and φ the time-independent parameters. Equation (1) would be simplified as $H = \frac{1}{2}\Omega(t)e^{i\varphi_1}|b\rangle\langle r| + \text{H.c.}$ in which we set the bright state $|b\rangle = \sin(\xi/2)e^{i\varphi}|0\rangle - \cos(\xi/2)|1\rangle$ and the dark state $|d\rangle = \cos(\xi/2)|0\rangle + \sin(\xi/2)e^{-i\varphi}|1\rangle$. By the requirement that the Hamiltonian H satisfies the Schrödinger equation $i\partial_t|\Psi(t)\rangle = H|\Psi(t)\rangle$ to inversely engineer the driving Hamiltonian [76], $|\Psi(t)\rangle$ in the subspace $\{|b\rangle, |r\rangle\}$ could be set as

$$|\Psi(t)\rangle = e^{-if(t)/2}\begin{pmatrix}\cos\frac{\Theta(t)}{2}e^{-i\alpha(t)/2}\\ \sin\frac{\Theta(t)}{2}e^{i\alpha(t)/2}\end{pmatrix}, \quad (2)$$

in which $\Theta(t), \alpha(t)$ are two time-dependent angles and $f(t)$ is a parameterized phase, which will be determined below. Inserting Eqs. (1) and (2) into the Schrödinger equation, we can obtain the following constraint relations of the parameters:

$$\begin{aligned}\dot{\Theta}(t) &= -\Omega(t)\sin[\alpha(t) + \varphi_1],\\ \dot{\alpha}(t) &= -\Omega(t)\cot\Theta(t)\cos[\alpha(t) + \varphi_1],\\ \dot{f}(t) &= -\dot{\alpha}(t)/\cos\Theta(t).\end{aligned} \quad (3)$$

That is, when the constraints of the parameters in Eq. (3) are satisfied, the system will evolve along with the state $|\Psi(t)\rangle$. To construct arbitrary geometric quantum gates based on a single-loop evolution in the computational basis $\{|0\rangle, |1\rangle\}$, $\Omega(t)$ and φ_1 of the Hamiltonian can be inversely determined from Eq. (3) as follows:

$$\begin{aligned}\varphi_1 &= \arctan[\dot{\Theta}(t)\cot\Theta(t)/\dot{\alpha}(t)] - \alpha(t),\\ \Omega(t) &= -\dot{\Theta}(t)/\sin[\alpha(t) + \varphi_1],\end{aligned} \quad (4)$$

and the boundary condition $\cos\Theta(0) = \cos\Theta(\tau) = 1$ needs to be satisfied to achieve a cyclic evolution where τ is the total operation time. A set of functions of Θ, α, and f can be selected for the cyclic boundary condition and constraints of Eq. (3), one simple choice is to set $\Theta = \pi\sin^2(\pi t/\tau)$ to satisfy the cyclic evolution condition. Moreover, to ensure that the full phase of the cyclic evolution has pure geometric properties, the control pulses and the state $|\Psi(t)\rangle$ are required to satisfy the following condition:

$$\int_0^\tau \langle\Psi(t)|H(t)|\Psi(t)\rangle dt = 0. \quad (5)$$

To satisfy the condition in Eq. (5), we consider dividing the physical procedure into two time intervals. In the first interval $t \in [0, \tau/2]$, we set $f = [2\Theta - \sin(2\Theta)]/4$, $\alpha = -\int \dot{f}\cos\Theta dt$, the evolution state will be spanned in the computation basis $\{|0\rangle, |1\rangle\}$. Thus, the corresponding evolution

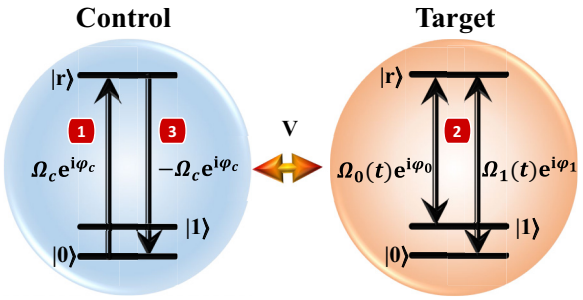

FIG. 1. Schematic of atomic levels and steps for constructing the nontrivial two-qubit geometric gate. In the ^{87}Rb atom, $|0\rangle$ and $|1\rangle$ are two hyperfine-Zeeman ground states and $|r\rangle$ is the Rydberg state. The transition $|0\rangle_c \to |r\rangle_c$ of the control atom is resonantly coupled to external laser with Rabi frequency $\Omega_c e^{i\varphi_c}$, while the transitions $|0\rangle_t \to |r\rangle_t$ ($|1\rangle_t \to |r\rangle_t$) of target atom are induced by the external lasers with Rabi frequency $\Omega_0(t)e^{i\varphi_0}$ [$\Omega_1(t)e^{i\varphi_1}$].

operator can be written as

$$U_1(\tau/2,0) = |d\rangle\langle d| + |\Psi(\tau/2)\rangle\langle\Psi(0)| = |d\rangle\langle d| + e^{i\gamma_1}|r\rangle\langle b|. \quad (6)$$

In the second interval $t \in [\tau/2, \tau]$, we set $f = [2\Theta - \sin(2\Theta)]/4$, $\alpha = -\int \dot{f}\cos\Theta dt - \gamma$ in which γ is an arbitrary constant. The resulting evolution operator is

$$U_2(\tau,\tau/2) = |d\rangle\langle d| + |\Psi(\tau)\rangle\langle\Psi(\tau/2)| = |d\rangle\langle d| + e^{i\gamma_2}|b\rangle\langle r|. \quad (7)$$

Thus, the final evolution operator is $U(\tau,0) = |d\rangle\langle d| + \Psi(\tau)\rangle\langle\Psi(0)| = |d\rangle\langle d| + e^{i(\gamma_1+\gamma_2)}|b\rangle\langle b|$, and after completing the systematic evolution, the dynamical phase can be eliminated by the mutation of the angle α in $t = \tau/2$, thus, we can obtain the arbitrary single-qubit Rydberg gate with pure geometric properties in the computational basis $\{|0\rangle, |1\rangle\}$

$$\begin{aligned} U(\gamma,\xi,\varphi) &= |d\rangle\langle d| + e^{i\gamma}|b\rangle\langle b| \\ &= e^{i\frac{\gamma}{2}}\begin{pmatrix} \cos\frac{\gamma}{2} - i\cos\xi\sin\frac{\gamma}{2} & -ie^{i\varphi}\sin\xi\sin\frac{\gamma}{2} \\ -ie^{-i\varphi}\sin\xi\sin\frac{\gamma}{2} & \cos\frac{\gamma}{2} + i\cos\xi\sin\frac{\gamma}{2} \end{pmatrix} \\ &= e^{i\frac{\gamma}{2}}e^{-i\frac{\gamma}{2}\boldsymbol{n}\cdot\boldsymbol{\sigma}}, \end{aligned} \quad (8)$$

in which $\gamma = \gamma_1 + \gamma_2$, $\boldsymbol{\sigma} = (\sigma_x, \sigma_y, \sigma_z)$ are standard Pauli matrices, $\boldsymbol{n} = (\sin\xi\cos\varphi, -\sin\xi\sin\varphi, \cos\xi)$, and the evolution operator $U(\gamma,\xi,\varphi)$ rotates around the axis $\boldsymbol{n}$ by an angle γ. For instance, when $\gamma = \pi, \xi = \pi/4, \varphi = 0$, U should be a Hadamard gate, while $\gamma = \pi, \xi = \pi/2, \varphi = 0$, U becomes a geometric NOT gate based on the Rydberg atom.

B. Nontrivial two-qubit geometric gate

The model for preparing the nontrivial two-qubit geometric gate is shown in Fig. 1. There are two Rydberg atoms which are identical to the atom that constructs the single-qubit geometric gate. Each atom possesses two hyperfine-Zeeman ground states $|0\rangle, |1\rangle$, and one Rydberg state $|r\rangle$. The interaction Hamiltonian between the two Rydberg atoms is $H_r = V|rr\rangle\langle rr|$ in which V is the van der Waals (vdW) interaction strength. $|0\rangle_c$ ($|1\rangle_c$) and $|0\rangle_t$ ($|1\rangle_t$) are coupled to $|r\rangle_c$ and $|r\rangle_t$ with Rabi frequencies $\Omega_{0c}(t)e^{i\varphi_{0c}}$ [$\Omega_{1c}(t)e^{i\varphi_{1c}}$] and $\Omega_{0t}(t)e^{i\varphi_{0t}}$ [$\Omega_{1t}(t)e^{i\varphi_{1t}}$], respectively, in which φ_{0c}, φ_{1c}, φ_{0t}, and φ_{1t} are time-independent laser phases. The subscript "c" ("t") denotes the control (target) atom. The parameters of the target atom are the same as those of the single Rydberg atom in the single-qubit gate of Sec. II A, i.e., $\Omega_{0t}(t) = \Omega_0(t)$, $\Omega_{1t}(t) = \Omega_1(t)$, $\varphi_{0t} = \varphi_0$, $\varphi_{1t} = \varphi_1$, $\Omega = \sqrt{\Omega_0^2 + \Omega_1^2}$, $\tan\xi/2 = -\Omega_0/\Omega_1$, and $\varphi = \varphi_0 - \varphi_1$. Thus, the Hamiltonian of the control and target atoms could be described by Eq. (1).

Next, as presented in Fig. 1, we show the construction method of the two-qubit geometric gate in the following three steps.

Step (i). We let $\Omega_{0c} = \Omega_c$ and simplify $\Omega_{1c} = 0$, $\varphi_{0c} = \varphi_c$. Under the condition, the Hamiltonian of the control atom is simplified as

$$H_c = \frac{1}{2}\Omega_c(t)|0\rangle_c\langle r|e^{i\varphi_c} + \text{H.c.}, \quad (9)$$

if we still set the same $|\Psi(t)\rangle$ as in Eq. (2). Inserting the $|\Psi(t)\rangle$ and the Hamiltonian of Eq. (9) into the Schrödinger equation, we will obtain the same constraints as Eq. (4), i.e., $\varphi_c = \arctan(\dot{\Theta}_c\cot\Theta_c/\dot{\alpha}_c) - \alpha_c$, $\Omega_c = -\dot{\Theta}_c/\sin(\alpha_c + \varphi_c)$.

Then we turn on the external laser acting on the control atom. The evolution operation can be written as $U_1 = |1\rangle_c\langle 1| + e^{i\gamma_{1c}}|r\rangle_c\langle 0|$. If the control atom is initially in the state $|0\rangle_c$, at $t = \tau/2$, the control atom will be excited to $|r\rangle_c$.

Step (ii). Carry out the single-qubit geometric operations on the target atom as shown in Sec. II A. The process is divided into two cases. For the target atom, one case is that, if the initial state of the control atom is $|1\rangle_c$, it should not be excited to $|r\rangle_c$ after step (i). The same unitary operator $U_t = e^{i\frac{\gamma_t}{2}}e^{-i\frac{\gamma_t}{2}\boldsymbol{n}\cdot\boldsymbol{\sigma}}$ as in Eq. (8) will be achieved for the target atom in which $\boldsymbol{n} = (\sin\xi\cos\varphi, -\sin\xi\sin\varphi, \cos\xi)$. The other case is that, if the initial state of the control atom is $|0\rangle_c$, it should be excited to $|r\rangle_c$ after step (i) and the target atom would perform nothing due to the Rydberg blockade effect where the condition $V \gg \Omega$ is satisfied. After the first two steps, we can obtain the evolution operator $U_2 = |1\rangle_c\langle 1| \otimes U_t + |r\rangle_c\langle r| \otimes I_t$.

Step (iii). Turn on the external laser acting on the control atom to perform the same operation as in Sec. II A; $|r\rangle_c$ is deexcited to $|0\rangle_c$ after the time $\tau/2$. The evolution operation is described as $U_3 = |1\rangle_c\langle 1| + e^{i\gamma_{2c}}|0\rangle_c\langle r|$.

Here we select the function of the parameters of the control and target atoms as

$$\begin{aligned} \Theta_c &= \begin{cases} \pi\sin^2\left(\frac{\pi t}{\tau}\right), & 0 \leqslant t \leqslant \tau/2, \\ \pi\sin^2\left(\frac{\pi(t-\tau)}{\tau}\right), & 3\tau/2 \leqslant t \leqslant 2\tau, \end{cases} \\ \alpha_c &= \begin{cases} -\int \dot{f}_c\cos\Theta_c dt, & 0 \leqslant t \leqslant \tau/2, \\ -\int \dot{f}_c\cos\Theta_c dt - \gamma_c, & 3\tau/2 \leqslant t \leqslant 2\tau, \end{cases} \\ \Theta_t &= \begin{cases} \pi\sin^2\left(\frac{\pi(t-\tau/2)}{\tau}\right), & \tau/2 \leqslant t \leqslant \tau, \\ \pi\sin^2\left(\frac{\pi(t-\tau/2)}{\tau}\right), & \tau \leqslant t \leqslant 3\tau/2, \end{cases} \\ \alpha_t &= \begin{cases} -\int \dot{f}_t\cos\Theta_t dt, & \tau/2 \leqslant t \leqslant \tau, \\ -\int \dot{f}_t\cos\Theta_t dt - \gamma_t, & \tau \leqslant t \leqslant 3\tau/2, \end{cases} \end{aligned} \quad (10)$$

and $f_c(t) = \{2\Theta_c(t) - \sin[2\Theta_c(t)]\}/4$. After these three steps, the final nontrivial two-qubit geometric gate is $U = U_3U_2U_1 = |1\rangle_c\langle 1| \otimes U_t + e^{i\gamma_c}|0\rangle_c\langle 0| \otimes I_t$ in which $\gamma_c = \gamma_{1c} + \gamma_{2c}$, $U_t = e^{i\frac{\gamma_t}{2}}e^{-i\frac{\gamma_t}{2}\boldsymbol{n}\cdot\boldsymbol{\sigma}}$. With the choice of $\gamma_c = 0$ and $\gamma_t = \pi$, the nontrivial two-qubit geometric gate in the

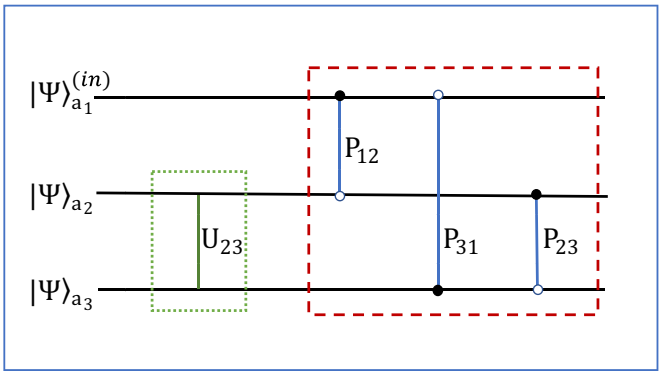

FIG. 2. Graphical representation of cloning machine circuit. The green dotted rectangle represents the controlled arbitrary nonadiabatic geometric quantum gate U_{23}, in which the green solid ball is the control qubit. The red dashed rectangle indicates three CNOT gates P_{12}, P_{31}, and P_{23}, in which • and ○ denote control qubit and target qubit, respectively. $|\Psi\rangle_{a_1}^{\text{in}}$, $|\Psi\rangle_{a_2}$, and $|\Psi\rangle_{a_3}$ are the initial states of three Rydberg atoms.

computation basis $\{|00\rangle, |01\rangle, |10\rangle, |11\rangle\}$ can be simplified as

$$U = \begin{pmatrix} 1 & 0 & 0 & 0 \\ 0 & 1 & 0 & 0 \\ 0 & 0 & \cos\xi & \sin\xi e^{i\varphi} \\ 0 & 0 & \sin\xi e^{-i\varphi} & -\cos\xi \end{pmatrix}. \tag{11}$$

The pure geometric properties of the two-qubit gate are still valid. First, the same as in the process of Sec. II A, the evolution of the target atom in step (ii) is purely geometric. Second, although they are not satisfied for the control atom in steps (i) or (iii), the cyclic evolution condition and the condition that accumulates the dynamic phase being zero still hold up when combining steps (i) and (iii) as a whole. In Sec. III, we discuss how to construct the cloning framework in Ref. [18] based on the unitary operation in Eq. (11).

III. IMPLEMENTATION OF QUANTUM CLONING MACHINE

In this section, the specific implementation process for different types of quantum cloning based on controlled two-qubit geometric quantum gates obtained in the previous section is described. The circuit for the realization of the cloning quantum state is demonstrated in Fig. 2.

Qubit a_1 (the state of atom 1) to be cloned is prepared in the state $|\Psi\rangle_{a_1}^{\text{in}}$,

$$|\Psi\rangle_{a_1}^{\text{in}} = \cos\frac{\theta}{2}|0\rangle_1 + e^{i\phi}\sin\frac{\theta}{2}|1\rangle_1, \tag{12}$$

in which $\theta \in [0, \pi]$ and $\phi \in [0, 2\pi]$. Initially, the states of atoms 2 and 3 (corresponding to qubits a_2 and a_3) are $|\Psi\rangle_{a_2}$ and $|\Psi\rangle_{a_3}$, respectively,

$$|\Psi\rangle_{a_2} = \cos\theta_1|0\rangle_2 + \sin\theta_1|1\rangle_2, \tag{13}$$

$$|\Psi\rangle_{a_3} = \cos\theta_2|0\rangle_3 + \sin\theta_2|1\rangle_3. \tag{14}$$

Let us consider the preparation process. Firstly perform the controlled arbitrary nonadiabatic geometric quantum gate Eq. (11) (with the choice of $\varphi = 0$ and for simplicity we let $\xi = \theta_3$) on qubits a_2 and a_3, that is to say, in the computational basis $\{|00\rangle_{23}, |01\rangle_{23}, |10\rangle_{23}, |11\rangle_{23}\}$,

$$U_{23} = \begin{pmatrix} 1 & 0 & 0 & 0 \\ 0 & 1 & 0 & 0 \\ 0 & 0 & \cos\theta_3 & \sin\theta_3 \\ 0 & 0 & \sin\theta_3 & -\cos\theta_3 \end{pmatrix}. \tag{15}$$

As shown in the green rectangle of the quantum circuit diagram in Fig. 2, after operating U_{23} on the qubits a_2 and a_3, the following evolution can be obtained [18]:

$$\begin{aligned} |\Psi\rangle_{23} &= U_{23}|\Psi\rangle_{a_2} \otimes |\Psi\rangle_{a_3} \\ &= P_1|00\rangle_{23} + P_2|01\rangle_{23} \\ &\quad + P_3|10\rangle_{23} + P_4|11\rangle_{23}, \end{aligned} \tag{16}$$

in which the coefficients P_i $(i = 1, 2, 3, 4)$ are

$$\begin{aligned} P_1 &= \cos\theta_1\cos\theta_2, \\ P_2 &= \cos\theta_1\sin\theta_2, \\ P_3 &= \sin\theta_1\cos(\theta_3 - \theta_2), \\ P_4 &= \sin\theta_1\sin(\theta_3 - \theta_2). \end{aligned} \tag{17}$$

Accordingly, the system state is

$$\begin{aligned} |\Psi\rangle_{a_1a_2a_3} &= |\Psi\rangle_{a_1}^{in} \otimes |\Psi\rangle_{23} \\ &= \cos\frac{\theta}{2}(P_1|000\rangle + P_2|001\rangle + p_3|010\rangle \\ &\quad + P_4|011\rangle) + e^{i\phi}\sin\frac{\theta}{2}(P_1|100\rangle \\ &\quad + P_2|101\rangle + P_3|110\rangle + P_4|111\rangle). \end{aligned} \tag{18}$$

Based on Eq. (11), with the choice of $\xi = \pi/2$, $\varphi = 0$, the CNOT gate can be constructed. Then we perform three CNOT operations P_{23}, P_{31}, and P_{12} on $|\Psi\rangle_{a_1a_2a_3}$, as shown in the red rectangle of the quantum circuit diagram in Fig. 2. We can obtain the following transformation:

$$\begin{aligned} |\Psi\rangle_{123} &= P_{23}P_{31}P_{12}|\Psi\rangle_{a_1a_2a_3} \\ &= \cos\frac{\theta}{2}[P_1|000\rangle + (P_3|01\rangle + P_2|10\rangle)|1\rangle \\ &\quad + P_4|110\rangle] + e^{i\phi}\sin\frac{\theta}{2}[P_1|111\rangle + (P_3|10\rangle \\ &\quad + P_2|01\rangle)|0\rangle + P_4|001\rangle]. \end{aligned} \tag{19}$$

The cloning machine with different types can be implemented in the framework Eq. (19) by properly adjusting the rotated angle θ_i $(i = 1, 2, 3)$.

After the cloning stage, the reduced density operators of qubits a_1, a_2, and a_3 are given as

$$\begin{aligned} \rho_1^{\text{out}} &= \text{Tr}_{a_2a_3}(|\Psi\rangle_{123}\langle\Psi|) = \Sigma_{i=1}^4|\Phi_i\rangle_{a_1}\langle\Phi_i|, \\ \rho_2^{\text{out}} &= \text{Tr}_{a_1a_3}(|\Psi\rangle_{123}\langle\Psi|) = \Sigma_{i=1}^4|\Psi_i\rangle_{a_2}\langle\Psi_i|, \\ \rho_3^{\text{out}} &= \text{Tr}_{a_1a_2}(|\Psi\rangle_{123}\langle\Psi|) = \Sigma_{i=1}^4|\Xi_i\rangle_{a_3}\langle\Xi_i|, \end{aligned} \tag{20}$$

where

$$|\Phi_{m\mp1}\rangle_{a_1} = \cos\frac{\theta}{2}P_{m\mp1}|0\rangle_1 + e^{i\phi}\sin\frac{\theta}{2}P_{m\pm1}|1\rangle_1,$$

$$|\Psi_{j+l}\rangle_{a_2} = \cos\frac{\theta}{2}P_{j+l}|0\rangle_2 + e^{i\phi}\sin\frac{\theta}{2}P_{\bar{j}+l}|1\rangle_2,$$
$$|\Xi_{p+l}\rangle_{a_3} = \cos\frac{\theta}{2}P_{p+l}|0\rangle_3 + e^{i\phi}\sin\frac{\theta}{2}P_{\bar{p}+\bar{l}}|1\rangle_3,$$
$$m = 2,3; j = 1,2; l = 0,2; p = 1,2. \quad (21)$$

In Eq. (21), the value of $\{\bar{j},\bar{l},\bar{p}\}$ is opposite to $\{j,l,p\}$. For instance, $\bar{j}$ takes 2 when j takes 1. The corresponding fidelity of $\rho_i^{(\text{out})}$ $(i=1,2,3)$ and $|\Psi\rangle_{a_1}^{(\text{in})}$ can be described as

$$F_1 = {}_{a_1}^{(\text{in})}\langle\Psi|\rho_1^{(\text{out})}|\Psi\rangle_{a_1}^{(\text{in})}$$
$$= P_1^2 + P_3^2 + \frac{\sin^2\theta}{2}\big[P_2^2 + P_4^2 - (P_1 - P_3)^2$$
$$+(e^{2i\phi} + e^{-2i\phi})P_2P_4\big], \quad (22)$$

and

$$F_2 = {}_{a_1}^{(\text{in})}\langle\Psi|\rho_2^{(\text{out})}|\Psi\rangle_{a_1}^{(\text{in})}$$
$$= P_1^2 + P_2^2 + \frac{\sin^2\theta}{2}\big[P_3^2 + P_4^2 - (P_1 - P_2)^2$$
$$+(e^{2i\phi} + e^{-2i\phi})P_3P_4\big], \quad (23)$$

and

$$F_3 = {}_{a_1}^{(\text{in})}\langle\Psi|\rho_3^{(\text{out})}|\Psi\rangle_{a_1}^{(\text{in})}$$
$$= P_1^2 + P_3^2 + \frac{\sin^2\theta}{2}\big[P_3^2 + P_2^2 - (P_1 - P_4)^2$$
$$+(e^{2i\phi} + e^{-2i\phi})P_2P_3\big]. \quad (24)$$

Then, the implementation methods for different types of cloning machines based on the framework in Eq. (19) are described in detail.

A. Implementation of 1 → 2 UQCM

To realize $1 \to 2$ UQCM, the fidelities of Eqs. (22) and (23) must be independent of ϕ and θ and the following conditions must be satisfied: $P_4 = 0$ and $P_1 = P_2 + P_3$. Accordingly, the three rotated angles are in the following relations: $\theta_2 = \theta_3$ and $\sin\theta_2 + \tan\theta_1 = \cos\theta_2$. Combiningthe above conditions and the unitary transformation in protocol [34], the transformation of optimal $1 \to 2$ asymmetrical UQCM (AUQCM) of our scheme can be written as

$$U_{\text{AUQCM}}|\Psi\rangle_{a_1}^{(\text{in})}|\Psi\rangle_{a_2}|\Psi\rangle_{a_3}$$
$$= \frac{\cos\frac{\theta}{2}}{\sqrt{1+p^2+q^2}}[|000\rangle + (p|01\rangle + q|10\rangle)|1\rangle]$$
$$+\frac{e^{i\phi}\sin\frac{\theta}{2}}{\sqrt{1+p^2+q^2}}[|111\rangle + (p|10\rangle + q|01\rangle)|0\rangle], \quad (25)$$

where $1/\sqrt{1+p^2+q^2} = \cos\theta_1\cos\theta_2$, $p = \tan\theta_1/\cos\theta_2$, and $q = \tan\theta_2$. Under these constraints, the ranges of the rotated angles θ_1 and θ_2 are changed to $\theta_1 \in [0, \arctan\sqrt{(\sqrt{5}-1)/\sqrt{2}}]$, $\theta_2 \in [0, \pi/4]$. The fidelities of the two clones of AUCQM can be rewritten as

$$F_1 = \frac{1+p^2}{1+p^2+q^2}, \quad F_2 = \frac{1+q^2}{1+p^2+q^2}. \quad (26)$$

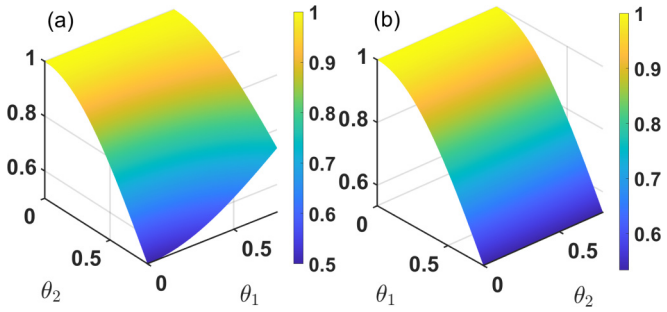

FIG. 3. (a) Fidelity F_1 of $1 \to 2$ AUQCM as function of θ_1 and θ_2, $\theta_1 \in [0, \arctan\sqrt{(\sqrt{5}-1)/\sqrt{2}}]$, $\theta_2 \in [0, \pi/4]$. (b) Fidelity F_2 of $1 \to 2$ AUQCM as function of θ_1 and θ_2, $\theta_1 \in [0, \arctan\sqrt{(\sqrt{5}-1)/\sqrt{2}}]$, $\theta_2 \in [0, \pi/4]$. F_1 and F_2 are the two analytical fidelities of $1 \to 2$ AUQCM in Eq. (26).

For $1 \to 2$ AUQCM, we plot the analytic diagram of Eq. (26) shown in Figs. 3(a) and 3(b) under these limitations $\theta_1 \in [0, \arctan\sqrt{(\sqrt{5}-1)/\sqrt{2}}]$, $\theta_2 \in [0, \pi/4]$. When $\theta_1 = \arctan(1/\sqrt{5})$ and $\theta_2 = \arctan(1/2)$, the corresponding fidelites F_1 and F_2 of SUQCM are $5/6$.

If the rotated angles are chosen as $\theta_1 \equiv \arctan 1/\sqrt{5}$ and $\theta_2 \equiv \arctan 1/2$, accordingly, $p = q = 1/2$ and $F_1 = F_2 = 5/6 \approx 0.8333$, the optimal AUQCM can be transformed to optimal symmetrical UQCM (SUQCM)

$$U_{\text{SUQCM}}|\Psi\rangle_{a_1}^{(\text{in})}|\Psi\rangle_{a_2}|\Psi\rangle_{a_3}$$
$$= \cos\frac{\theta}{2}\left[\sqrt{\frac{2}{3}}|000\rangle + \sqrt{\frac{1}{6}}(|01\rangle + |10\rangle)|1\rangle\right]$$
$$+e^{i\phi}\sin\frac{\theta}{2}\left[\sqrt{\frac{2}{3}}|111\rangle + \sqrt{\frac{1}{6}}(|10\rangle + |01\rangle)|0\rangle\right]. \quad (27)$$

The robustness against dissipation and control error for the $1 \to 2$ SUQCM is considered in the next section via numerical simulation of the master equation.

B. Implementation of PCCM

Based on the framework shown in Eq. (19), we can implement $1 \to 2$ PCCM if the amplitude of $|\Psi\rangle_{a_1}^{\text{in}}$ is given, i.e., θ is known, accordingly, the fidelities of Eqs. (22) and (23) only need to be phase (ϕ) independent and the proper parameters must be selected to satisfy $P_4 = 0$. Based on Eq. (17) the parameter condition $\theta_2 = \theta_3$ can be easily deduced.

If the input state to be cloned is $|\Psi\rangle_{a_1}^{(\text{in})} = |\Psi\rangle_E^{xy} = 1/\sqrt{2}|0\rangle_1 + e^{i\phi}1/\sqrt{2}|1\rangle_1$, which corresponds to the x-y plane equatorial vector of the Bloch sphere. For the present scheme, if the parameters satisfy the conditions $\theta_2 = \theta_3$ and $\cos\theta_1\cos\theta_2 = 1/\sqrt{2}$, the cloning transformation reduces to the optimal $1 \to 2$ asymmetrical PCCM (APCCM)

$$U_{\text{APCCM}}|\Psi\rangle_E^{xy}|\Psi\rangle_{a_2}|\Psi\rangle_{a_3}$$
$$= \{[|000\rangle + (\cos\varpi|01\rangle + \sin\varpi|10\rangle)|1\rangle]/\sqrt{2}$$
$$+e^{i\phi}[|111\rangle + (\cos\varpi|10\rangle + \sin\varpi|01\rangle)|0\rangle]/\sqrt{2}\}/\sqrt{2}. \quad (28)$$

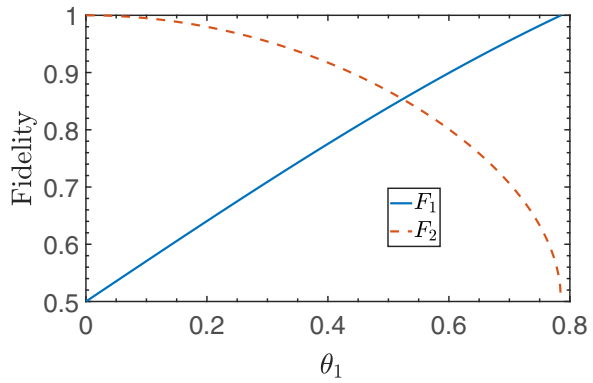

FIG. 4. Analytical values of fidelities F_1 and F_2 for $1 \to 2$ APCCM versus θ_1, with the parameters $\theta = \pi/2$, $\theta_2 = \theta_3$ and $\cos\theta_1 \cos\theta_2 = 1/\sqrt{2}$.

According to Eqs. (17), (19), and Eq. (28), we can obtain $\cos\varpi = \sqrt{2}\sin\theta_1$ and $\sin\varpi = \sqrt{2\cos^2\theta_1 - 1}$ in which $\theta_1, \theta_2 \in [0, \pi/4]$, and $\varpi \in [0, \pi/2]$. We can calculate the fidelity of the APCCM

$$F_1 = (1 + \cos\varpi)/2, \quad F_2 = (1 + \sin\varpi)/2. \tag{29}$$

For $1 \to 2$ APCCM, according to the analytic fidelity equation (29) with the condition $\theta_1 \in [0, \pi/4]$, we plot the diagram as shown in Fig. 4. When we choose $\theta_1 = \pi/6$ and $\theta_2 = \arccos\sqrt{2/3}$, the fidelities reduce to $F_1 = F_2 = 1/2(1 + 1/\sqrt{2}) \approx 0.8536 > 0.8333$, which also confirms the fact that, because some information of the state cloned by PCCM is known in advance, the fidelity of the copy cloned by SPCCM should be higher than that of SUQCM.

If we choose $\theta_1 \equiv \pi/6$ and $\theta_2 \equiv \arccos\sqrt{2/3}$, the fidelities reduce to $F_1 = F_2 = 1/2(1 + 1/\sqrt{2}) \approx 0.8536$ and the optimal $1 \to 2$ APCCM is transformed to optimal $1 \to 2$ symmetrical PCCM (SPCCM)

$$\begin{aligned} &U_{\mathrm{SPCCM}}|\Psi\rangle_E^{xy}|\Psi\rangle_{a_2}|\Psi\rangle_{a_3} \\ &= \frac{1}{2}|000\rangle + \frac{1}{2\sqrt{2}}(|01\rangle + |10\rangle)|1\rangle \\ &\quad + e^{i\phi}\left[\frac{1}{2}|111\rangle + \frac{1}{2\sqrt{2}}(|10\rangle + |01\rangle)|0\rangle\right]. \end{aligned} \tag{30}$$

The robustness against dissipation and control error for the $1 \to 2$ SPCCM is considered in the next section via numerical simulation of the master equation.

C. Implementation of RSCM

We also analyze the cloning transformation of the states corresponding to the x-z plane vectors on the Bloch sphere, namely RSCM. The azimuthal angle ϕ of the input state is 0 or π, accordingly, $|\Psi\rangle_{a_1}^{(\mathrm{in})} = |\Psi\rangle_E^{xz} = \cos\frac{\theta}{2}|0\rangle_1 \pm \sin\frac{\theta}{2}|1\rangle_1$. From Eqs. (22) and (23), the fidelities for the two copies in $1 \to 2$ RSCM can be derived as

$$\begin{aligned} F_1 &= P_1^2 + P_3^2 + \frac{\sin^2\theta}{2}[(P_2 + P_4)^2 - (P_1 - P_3)^2], \\ F_2 &= P_1^2 + P_2^2 + \frac{\sin^2\theta}{2}[(P_3 + P_4)^2 - (P_1 - P_2)^2]. \end{aligned} \tag{31}$$

As presented in Ref. [17], the solution $P_1 = P_2 + P_3 + P_4$ ensures that fidelities of $1 \to 2$ RSCM are independent of the input state. We can obtain

$$F_1 = P_1^2 + P_3^2, \quad F_2 = P_1^2 + P_2^2. \tag{32}$$

Considering $P_1 = P_2 + P_3 + P_4$, the normalization condition $P_1^2 + P_2^2 + P_3^2 + P_4^2 = 1$, and Eq. (32), we can calculate [17]

$$\begin{aligned} P_1 &= \frac{\sqrt{F_1 - 2\sqrt{F_1^3 - F_1^4}}\left(F_1 + 2\sqrt{F_1^3 - F_1^4}\right)}{\sqrt{2}F_1(2F_1 - 1)}, \\ P_2 &= \frac{F_1(2F_1 - 1)\left(F_1 - F_1^2 + \sqrt{F_1^3 - F_1^4}\right)}{\sqrt{2}\sqrt{F_1 - \sqrt{F_1^{3-2F_1^4}}}\left(F_1^2 + \sqrt{F_1^3 - F_1^4}\right)}, \\ P_3 &= \frac{1}{\sqrt{2}}\sqrt{F_1 - 2\sqrt{F_1^3 - F_1^4}}, \\ P_4 &= \frac{\sqrt{F_1^3 - F_1^4}\sqrt{F_1 - 2\sqrt{F_1^3 - F_1^4}}}{\sqrt{2}F_1^2}, \\ F_2 &= 1/2 + \sqrt{F_1(1 - F_1)}. \end{aligned} \tag{33}$$

Since the fidelities F_1 and F_2 are related to the three rotation angles θ_1, θ_2, and θ_3, the analytical value of the fidelity of the real-state cloning machine should not be plotted.

As long as the parameters meet the conditions of Eq. (33), the optimal $1 \to 2$ asymmetrical (symmetrical) RSCM can be realized. For the present protocol, we take an example: if we want to get $F_1 = 1, F_2 = 1/2$, the condition $\theta_1 = \pi/4, \theta_2 = \theta_3 = 0$ can be deduced.

However, there is an exception in the $1 \to 2$ asymmetrical RSCM (ARSCM) scheme. From P_1 of Eq. (33), we find that the value of $F_1 = 1/2$ cannot be obtained. In this case, as presented in Ref. [17], the relation $P_1 = P_2 = 1/\sqrt{2}$ and $P_3 = -P_4 = 0$ can maintain the validity of the protocol, that is to say $\theta_1 = 0, \theta_2 = \pi/4$, and the corresponding fidelity values are $F_1 = 1/2, F_2 = 1$.

For $1 \to 2$ symmetrical RSCM (SRSCM), we set $\theta_1 \equiv \theta_2 \equiv \pi/8$ and $\theta_3 = \pi/4$ and the optimal $1 \to 2$ SRSCM can be implemented as follows:

$$\begin{aligned} &U_{\mathrm{SRSCM}}|\Psi\rangle_E^{xz}|\Psi\rangle_{a_2}|\Psi\rangle_{a_3} \\ &= \cos\frac{\theta}{2}\left[\left(\frac{1}{2} + \frac{1}{\sqrt{8}}\right)|000\rangle + \frac{1}{2}|+\rangle|1\rangle\right. \\ &\quad \left. + \left(\frac{1}{2} - \frac{1}{\sqrt{8}}\right)|110\rangle\right] + \sin\frac{\theta}{2}\left[\left(\frac{1}{2} + \frac{1}{\sqrt{8}}\right)|111\rangle\right. \\ &\quad \left. + \frac{1}{2}|+\rangle|01\rangle + \left(\frac{1}{2} - \frac{1}{\sqrt{8}}\right)|001\rangle\right], \end{aligned} \tag{34}$$

where $|+\rangle = (|01\rangle + |10\rangle)/\sqrt{2}$. Accordingly, the fidelities of $1 \to 2$ SRSCM are $F_1 = F_2 = 1/2(1 + 1/\sqrt{2}) \approx 0.8536$, which are the same as that of $1 \to 2$ SPCCM. The robustness against dissipation and control error for the $1 \to 2$ SRSCM is considered in the next section via numerical simulation of the master equation.

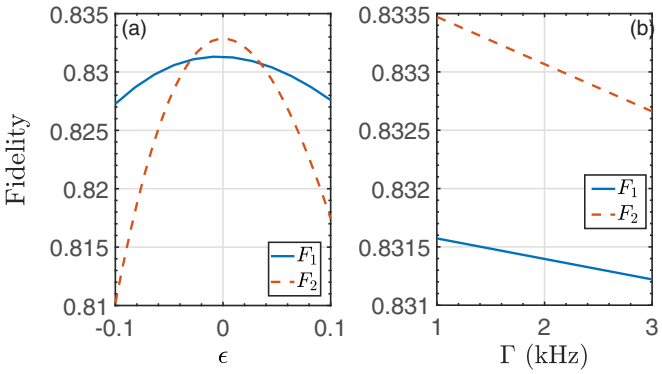

FIG. 5. (a) Fidelities of $1 \to 2$ SUQCM versus control erro ϵ. (b) Fidelities of $1 \to 2$ SUQCM versus decay Γ. The parameters are chosen as $\theta_1 = \arctan 1/\sqrt{5}$, $\theta_2 = \arctan 1/2$, θ and ϕ can take any value, we choose $\theta = \pi/3$ and $\phi = \pi/9$ for the numerical simulation. $\epsilon \in [-0.1, 0.1]$, $\Gamma \in [1, 3]$ kHz. Its dissipation dynamics is described by Eq. (36) with $\Omega_{\max} = 2\pi \times 10$ MHz and $V = 2\pi \times 249$ MHz.

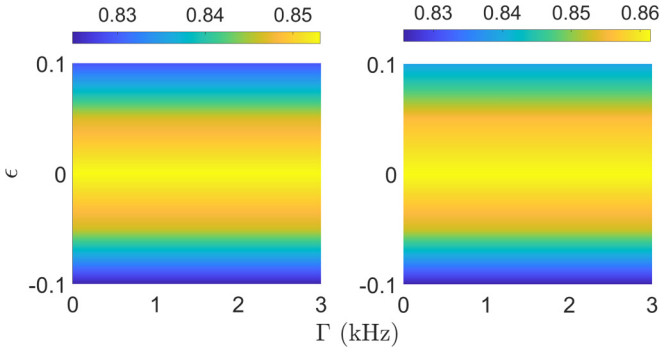

FIG. 6. (a) Fidelity F_1 of $1 \to 2$ SPCCM versus control error ϵ and decay Γ. (b) Fidelity F_2 of $1 \to 2$ SPCCM versus error ϵ and decay Γ. The parameters are chosen as $\theta = \pi/2$, $\theta_1 \equiv \pi/6$, and $\theta_2 \equiv \arccos\sqrt{2/3}$. ϕ can take any value, we choose $\phi = \pi/2$ for the numerical simulation, $\epsilon \in [-0.1, 0.1]$, $\Gamma \in [1, 3]$ kHz. Its dissipation dynamics is described by Eq. (36), with $\Omega_{\max} = 2\pi \times 10$ MHz and $V = 2\pi \times 249$ MHz.

With the choice of $\theta_1 = \arcsin 1/\sqrt{6}$, $\theta_2 = \arctan 1/3$, and $\theta_3 = \pi/4 + \arctan 1/3$ we can implement the optimal $1 \to 3$ SERSCM. The corresponding transformation form is

$$\begin{aligned} &U_{\text{SERSCM}}|\Psi\rangle_E^{xz}|\Psi\rangle_{a_2}|\Psi\rangle_{a_3} \\ &= \cos\frac{\theta}{2}\left[\frac{\sqrt{3}}{2}|000\rangle + \frac{1}{\sqrt{12}}(|001\rangle + |100\rangle + |110\rangle)\right] \\ &\quad + \sin\frac{\theta}{2}\left[\frac{\sqrt{3}}{2}|111\rangle + \frac{1}{\sqrt{12}}(|100\rangle + |010\rangle + |001\rangle)\right], \end{aligned} \tag{35}$$

with the fidelities of the three clones $F_1 = F_2 = F_3 = 5/6$.

IV. EFFECT OF DISSIPATION AND CONTROL ERROR ON THE FIDELITY OF QUANTUM CLONING MACHINE

In the present Rydberg cloning scheme based on the optimized NGQC, it is inevitable that the control error and the dissipation caused by atomic spontaneous emission should result insystem decoherence. Considering the spontaneous emission from highly excited states to ground states, the evolution of the system is governed by the Lindblad master equation

$$\begin{aligned} \dot{\rho}(t) = i[\rho(t), H(t)] + \frac{1}{2}\sum_l\sum_s \big[2\mathcal{L}_l^s\rho\mathcal{L}_l^{s\dagger} \\ - \big(\mathcal{L}_l^{s\dagger}\mathcal{L}_l^s\rho + \rho\mathcal{L}_l^{s\dagger}\mathcal{L}_l^s\big)\big], \end{aligned} \tag{36}$$

in which $\rho(t)$ is the density matrix of the systematic state, $H(t)$ is the Hamiltonian of the system, and $\mathcal{L}_l^s = \sqrt{\Gamma/2}|s\rangle_l\langle r|$ is the Lindblad operator with the subscript l labeling the lth atom and $s = 0, 1$ representing the two ground states. Here, for the ^{87}Rb atom, the Rydberg states are $|r\rangle_c = |r\rangle_t = |71s_{1/2}\rangle$. The C_6 parameter can be evaluated to be 1020 GHz μm^6 [77]. When two atoms are placed $d = 4\,\mu$m, the corresponding strength of the vdW interaction is $V = 2\pi \times 249$ MHz and $\Omega_{\max} = 2\pi \times 10$ MHz. The fidelity $F = |\langle\psi_{\text{ideal}}|\psi(t)\rangle|^2$ is used to estimate the effectiveness of the present cloning scheme, where $|\psi_{\text{ideal}}\rangle$ is the target state experiencing the ideal gate and $|\psi(t)\rangle$ is the state governed by the master equation in Eq. (36).

Next, we check the robustness against systematic error for the $1 \to 2$ SUQCM. The leading Hamiltonian would be $H'(t) = (1+\epsilon)H(t)$, where $H(t)$ is the ideal Hamiltonian and $\epsilon \in [-0.1, 0.1]$, which is regarded as slow quasistatic noise [78,79]. As shown in Figs. 5(a) and 5(b), we plot the fidelity of $1 \to 2$ SUQCM versus error ϵ and decay rate Γ, respectively, in which the decay rate $\Gamma \in [1, 3]$ kHz. It needs to be specifically pointed out that in Figs. 5–7 all control errors and decoherence are taken into account in the entire evolution process of the system (including U_{23} and three CNOT operations P_{12}, P_{31}, and P_{23}).

For $1 \to 2$ SPCCM and SRSCM, the same characteristics produced by geometric quantum computation are also present and the effects of systematic errors and decoherence are within our acceptable limits. In Figs. 6 and 7, we show the

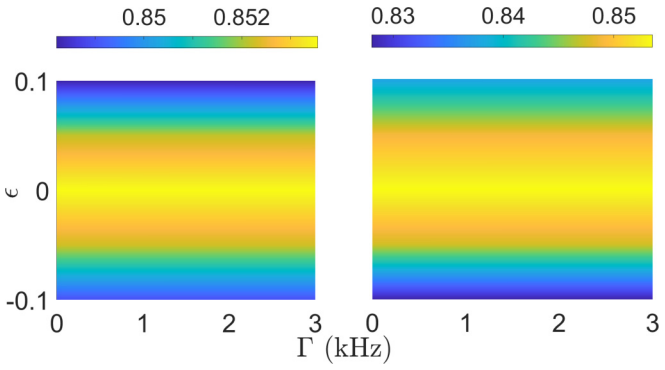

FIG. 7. (a) Fidelity F_1 of $1 \to 2$ SRSCM versus control error ϵ and decay Γ. (b) Fidelity F_2 of $1 \to 2$ SRSCM versus error ϵ and decay Γ. The parameters are chosen as $\phi = 0$, $\theta_1 = \theta_2 = \pi/8$, and $\theta_3 = \pi/4$. θ can take any value, we choose $\theta = \pi/3$ for the numerical simulation, $\epsilon \in [-0.1, 0.1]$, $\Gamma \in [1, 3]$ kHz. Its dissipation dynamics is described by Eq. (36), with $\Omega_{\max} = 2\pi \times 10$ MHz and $V = 2\pi \times 249$ MHz.

number fitting of $1 \rightarrow 2$ SPCCM and SRSCM against error ϵ and decay Γ, respectively. Meanwhile, the optimal fidelity is $F_1 = F_2 = 1/2(1 + 1/\sqrt{2}) \approx 0.8536$, which is the same for the SPCCM and SRSCM and higher than that of SUQCM under the case of no error and decoherence.

V. CONCLUSION

In summary, we propose a scheme for the construction of fast and robust quantum cloning machines. Using the Rydberg blockade mechanism and the optimized NGQC, we realize the two-qubit geometric gates. Based on the quantum circuit constructed by the two-qubit geometric gates, we implement the $1 \rightarrow 2$ symmetrical (asymmetrical) universal cloning, $1 \rightarrow 2$ optimal symmetrical (asymmetrical) phase-covariant quantum cloning, $1 \rightarrow 2$ optimal symmetrical (asymmetrical) real-state quantum cloning, and $1 \rightarrow 3$ symmetrical economical real-state quantum cloning. Through numerically simulating the fidelities of the cloning machine under control error and spontaneous emission, we confirm the feasibility of the Rydberg quantum cloning scheme. Therefore, our scheme may provide an alternative way to experimentally carry out simple and robust quantum cloning.

ACKNOWLEDGMENTS

The authors are grateful to Prof. X. K. Song, Dr. Li-Na Sun, and Lü-Yun Wang for valuable discussions on the manuscript. This work was supported by National Natural Science Foundation of China (Grants No. 12274376 and No. 12074346) and the Natural Science Foundation of Henan Province (Grant No. 212300410085). Major science and technology project of Henan Province (Grant No. 221100210400).

APPENDIX A: FIDELITIES OF THE GEOMETRIC QUANTUM GATES

In the geometric gates based on the Rydberg atomic system, their fidelity should inevitably be affected by the dissipation caused by spontaneous emission from highly excited states to ground states. The evolution process taking dissipation into account is governed by the Lindblad master equation in Eq. (36). Using the same atomic parameters as in Sec. IV, we estimate the experimental feasibility of the gates and present the numerical simulation of the fidelities of the NOT and CNOT gates. Moreover, assuming the initial state $|\psi(0)\rangle = \cos\chi|0\rangle + \sin\chi|1\rangle$, using the shape of $\Omega(t)$ and φ_1 shown in Fig. 8(a) with $\Omega_{\max} = 2\pi \times 10\,\mathrm{MHz}$, the decay rate $\Gamma = 2.5$ kHz [80] in Fig. 8(b), we present the numerical simulation of single-qubit NOT gate with the fidelity defined by $F = \frac{1}{2\pi}\int_0^{2\pi}\langle\psi|\rho(t)|\psi\rangle d\chi$ with the ideal final state $|\psi\rangle = U_{\mathrm{NOT}}|\psi(0)\rangle$. Moreover, with the same maximum value $\Omega_{\max} = 2\pi \times 10\,\mathrm{MHz}$, taking the two-qubit CNOT gate as an example, we use the fidelity $F = \frac{1}{(2\pi)^2}\int_0^{2\pi}\int_0^{2\pi}\langle\psi|\rho(t)|\psi\rangle d\chi_1 d\chi_2$ to evaluate the performance of the nonadiabatic geometric operation in which the initial state is $|\psi(0)\rangle = (\cos\chi_1|0\rangle_c + \sin\chi_1|1\rangle_c) \otimes (\cos\chi_2|0\rangle_t + \sin\chi_2|1\rangle_t)$. Meanwhile, the populations of the corresponding states in the evolution process are also given in Fig. 8. In Fig. 8(a), we take the single-qubit NOT gate and the two-qubit CNOT gate as examples, and in Fig. 8(a) we draw the change rule of the pulse envelope acting on the (target) qubit versus time. In addition, in Figs. 8(b) and 8(c), we show the populations of $\{|0\rangle, |1\rangle, |r\rangle, |00\rangle, |01\rangle, |10\rangle, |11\rangle\}$ of single(two)-qubit and the fidelities of the NOT gate and CNOT gate can reach 99.98% and 99.92%, respectively.

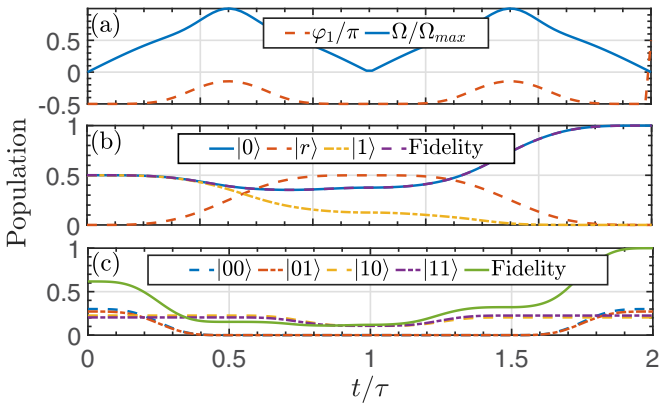

FIG. 8. (a) The Rabi frequency Ω and φ_1 versus t/τ for the NOT gate. The parameters are $\Omega_{\max} = 2\pi \times 10\,\mathrm{MHz}$ and $V = 2\pi \times 249\,\mathrm{MHz}$. Suppose the initial state is $|\psi(0)\rangle = \cos\chi|0\rangle + \sin\chi|1\rangle$. (b) Populations of $|0\rangle$, $|1\rangle$, and $|r\rangle$ in single qubit NOT qubit. (c) Populations of $|00\rangle$, $|01\rangle$, $|10\rangle$, and $|11\rangle$ in two-qubit gates CNOT. Suppose the system is initially in the state $|\psi(0)\rangle = (\cos\chi_1|0\rangle_c + \sin\chi_1|1\rangle_c) \otimes (\cos\chi_2|0\rangle_t + \sin\chi_2|1\rangle_t)$.

APPENDIX B: COMPARISON WITH THE SCHEME IN REF. [18]

Different types of quantum cloning machines were implemented by employing the interaction between electron-spin and the optical coherent pulse in Ref. [18]. If it was realized in the Rydberg atom, we can use laser drive to realize

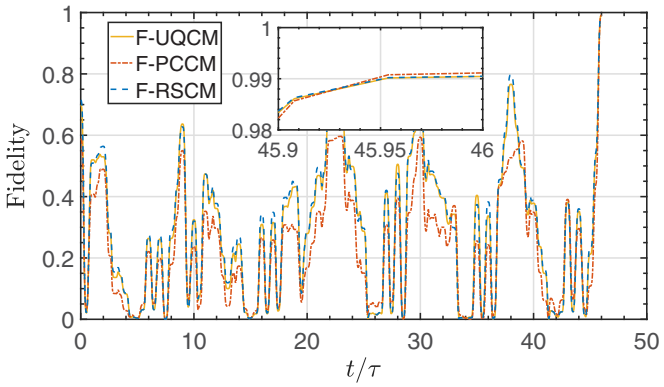

FIG. 9. The fidelities of the three-qubit entangled state in Eq. (19) versus t, in which $\tau = 22.214\,\mu\mathrm{s}$, $\Gamma = 2.5 \times 10^3$ kHz, $\Omega_{\max} = 2\pi \times 10\,\mathrm{MHz}$, and $V = 2\pi \times 249\,\mathrm{MHz}$. The input state to be cloned is $|\Psi\rangle_{a_1}^{\mathrm{in}} = \cos\theta/2|0\rangle_1 + e^{i\phi}\sin\theta/2|1\rangle_1$, for the UQCM, PCCM, and RSCM, the corresponding parameters are $(\theta = \pi/3, \phi = \pi/9)$, $(\theta = \pi/2, \phi = \pi/8)$, and $(\theta = \pi/3, \phi = 0)$, respectively. The cloning framework in Eq. (19) is obtained by repeating all of single- and two-qubit unitary operations in the order required by the cloning scheme in Ref. [18] in the Rydberg atom.

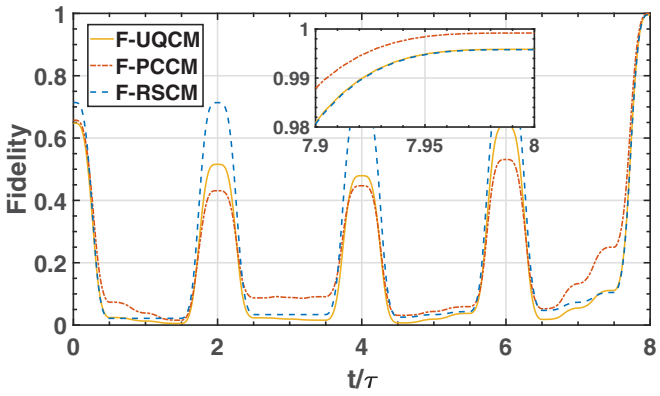

FIG. 10. The fidelities of the three-qubit entangled state in Eq. (19) versus t, in which $\tau = 22.214\,\mu$s, $\Gamma = 2.5 \times 10^3$ kHz, $\Omega_{\max} = 2\pi \times 10$ MHz, and $V = 2\pi \times 249$ MHz. The input state to be cloned is $|\Psi\rangle_{a_1}^{\text{in}} = \cos\theta/2|0\rangle_1 + e^{i\phi}\sin\theta/2|1\rangle_1$, for the UQCM, PCCM, and RSCM, the corresponding parameters are $(\theta = \pi/3, \phi = \pi/9)$, $(\theta = \pi/2, \phi = \pi/8)$, and $(\theta = \pi/3, \phi = 0)$, respectively. In our scheme, the cloning framework in Eq. (19) is achieved by directly constructing the unitary operation required by the cloning machine in the Rydberg atom based on the optimized NGQC.

the single(two)-qubit operations in their scheme. We can select different parameters based on Eq. (8) to realize some single-qubit and two-qubit operations of Ref. [18]. For example, when we constructed the cloning machine mentioned in Ref. [18] in the Rydberg atom, the U_{23} operation was realized by 15 single-qubit gates and 2 double-qubit gates (the quantum gate $e^{i\pi/4\sigma_{z2}\sigma_{z3}}$ required to construct U_{23} in Ref. [18] can be realized by the controlled-z geometric and single-qubit operation [81]). The three CNOT operations are realized through four single-qubit gates and one two-qubit gate, respectively.

In Fig. 9, in the Rydberg atom system, by repeating the unitary operation steps in Ref. [18], we plot the fidelities of the state in Eq. (19) for different input states to be cloned and we give the fidelities of the three-qubit entangled state required by the corresponding UQCM, PCCM, and RSCM; the values are 99.01%, 99.11%, and 99.05%, respectively. In our scheme, the cloning framework in Eq. (19) is achieved by directly constructing the unitary operation required by the cloning machine in the Rydberg atom based on the optimized NGQC. The fidelities of three-qubit entangled state required by the corresponding UQCM, PCCM, and RSCM are shown in Fig. 10: the values are 99.59%, 99.92%, and 99.58%, respectively.

Comparing Figs. 9 and 10, it is easy to see that our scheme based on the optimized NGQC direct implementation of the unitary operation required to build the cloning machine requires only 8τ compared to the 46τ required to repeat Ref. [18] in the Rydberg atom, which results in a higher fidelity of our scheme, as longer operation times inevitably lead to greater decoherence. The present scheme to optimize quantum cloning using geometric quantum control in Rydberg atoms provides a path to robust and simplified quantum cloning, which is meaningful for experiments and has implications for quantum cloning in other quantum systems as well.

[1] W. K. Wootters and W. H. Zurek, Nature (London) **299**, 802 (1982).
[2] V. Bužek and M. Hillery, Phys. Rev. A **54**, 1844 (1996).
[3] N. Gisin and S. Massar, Phys. Rev. Lett. **79**, 2153 (1997).
[4] D. Bruß, D. P. DiVincenzo, A. Ekert, C. A. Fuchs, C. Macchiavello, and J. A. Smolin, Phys. Rev. A **57**, 2368 (1998).
[5] N. Gisin, Phys. Lett. A **242**, 1 (1998).
[6] Y.-N. Wang, H.-D. Shi, Z.-X. Xiong, L. Jing, X.-J. Ren, L.-Z. Mu, and H. Fan, Phys. Rev. A **84**, 034302 (2011).
[7] D. Bruß, M. Cinchetti, G. M. D'Ariano, and C. Macchiavello, Phys. Rev. A **62**, 012302 (2000).
[8] N. J. Cerf, J. Mod. Opt. **47**, 187 (2000).
[9] H. Fan, K. Matsumoto, X.-B. Wang, and M. Wadati, Phy. Rev. A **65**, 012304 (2001).
[10] V. Karimipour and A. T. Rezakhani, Phys. Rev. A **66**, 052111 (2002).
[11] H. Fan, H. Imai, K. Matsumoto, and X. B. Wang, Phys. Rev. A **67**, 022317 (2003).
[12] F. Buscemi, G. M. D'Ariano, and C. Macchiavello, Phys. Rev. A **71**, 042327 (2005).
[13] W.-H. Zhang and L. Ye, New J. Phys. **9**, 318 (2007).
[14] K. Bartkiewicz, A. Miranowicz, and Ş. K. Özdemir, Phys. Rev. A **80**, 032306 (2009).
[15] L. Jing, Y.-N. Wang, H.-D. Shi, L.-Z. Mu, and H. Fan, Phys. Rev. A **86**, 062315 (2012).
[16] B.-L. Fang, Z. Yang, and L. Ye, Phys. Rev. A **79**, 054308 (2009).
[17] W.-H. Zhang, T. Wu, L. Ye, and J.-L. Dai, Phy. Rev. A **75**, 044303 (2007).
[18] M.-Z. Zhu and L. Ye, Phys. Rev. A **91**, 042319 (2015).
[19] P. Navez and N. J. Cerf, Phys. Rev. A **68**, 032313 (2003).
[20] S. Ghosh, G. Kar, and A. Roy, Phys. Lett. A **261**, 17 (1999).
[21] H. Barnum, C. M. Caves, C. A. Fuchs, R. Jozsa, and B. Schumacher, Phys. Rev. Lett. **76**, 2818 (1996).
[22] S.-L. Luo and W. Sun, Phys. Rev. A **82**, 012338 (2010).
[23] D. Bruß, Phys. Rev. Lett. **81**, 3018 (1998).
[24] A. H. Werner, T. Franz, and R. F. Werner, Phys. Rev. Lett. **103**, 220504 (2009).
[25] N. J. Cerf, M. Lévy, and G. Van Assche, Phys. Rev. A **63**, 052311 (2001).
[26] K. Bartiewicz, K. Lerm, A. Cernoch, J. Soubusta, and A. Miranowicz, Phys. Rev. Lett. **110**, 173601 (2013).
[27] A. Ferenczi and N. Lütkenhaus, Phys. Rev. A **85**, 052310 (2012).
[28] V. Bužek and M. Hillery, Phys. Rev. Lett. **81**, 5003 (1998).
[29] C.-S. Niu and R. B. Griffiths, Phys. Rev. A **58**, 4377 (1998).
[30] N. J. Cerf, Phys. Rev. Lett. **84**, 4497 (2000).
[31] S. L. Braunstein, V. Bužek, and M. Hillery, Phys. Rev. A **63**, 052313 (2001).
[32] S. Iblisdir, A. Acin, N. J. Cerf, R. Filip, J. Fiurasek, and N. Gisin, Phys. Rev. A **72**, 042328 (2005).

[33] A. Kay, R. Ramanathan, and D. Kaszlikowski, Quant. Inf. Comput. **13**, 880 (2013).

[34] I. Ghiu, Phys. Rev. A **67**, 012323 (2003).

[35] E. Nagali, D. Giovannini, L. Marrucci, S. Slussarenko, E. Santamato, and F. Sciarrino, Phys. Rev. Lett. **105**, 073602 (2010).

[36] L.-C. Peng, D. Wu, H.-S. Zhong, Y.-H. Luo, Y. Li, Y. Hu, X. Jiang, M.-C. Chen, L. Li, N.-L. Liu, K. Nemoto, W. J. Munro, B. C. Sanders, C.-Y. Lu, and J.-W. Pan, Phys. Rev. Lett. **125**, 210502 (2020).

[37] S. Liu, Y. Luo, Y. Chen, and J. Jing, Phys. Rev. Lett. **126**, 060503 (2021).

[38] Z.-B. Yang, P.-R. Han, X.-J. Huang, W. Ning, H. Li, K. Xu, D. Zheng, H. Fan, and S.-B. Zheng, npj Quantum Inf. **7**, 44 (2021).

[39] B. Coyle, M. Doosti, E. Kashefi, and N. Kumar, Phys. Rev. A **105**, 042604 (2022).

[40] M. Saffman, T. G. Walker, and K. Mølmer, Rev. Mod. Phys. **82**, 2313 (2010); H. Levine, A. Keesling, G. Semeghini, A. Omran, T. T. Wang, S. Ebadi, H. Bernien, M. Greiner, V. Vuletić, H. Pichler, and M. D. Lukin, Phys. Rev. Lett. **123**, 170503 (2019); S.-L. Su, Y. Gao, E.-J. Liang, and S. Zhang, Phys. Rev. A **95**, 022319 (2017); J.-Z. Xu, L.-N. Sun, J.-F. Wei, Y.-L. Du, R.-H. Luo, L.-L. Yan, M. Feng, and S.-L. Su, Chi. Phys. Lett. **39**, 090301 (2022); L.-N. Sun, F.-Q. Guo, Z. Shan, M. Feng, L.-L. Yan, S.-L. Su, Phys. Rev. A **105**, 062602 (2022).

[41] A. Gaëtan, Y. Miroshnychenko, T. Wilk, A. Chotia, M. Viteau, D. Comparat, P. Pillet, A. Browaeys, and P. Grangier, Nat. Phys. **5**, 115 (2009).

[42] E. Urban, T. A. Johnson, T. Henage, L. Isenhower, D. D. Yavuz, T. G. Walker, and M. Saffman, Nat. Phys. **5**, 110 (2009).

[43] D. Jaksch, J. I. Cirac, P. Zoller, S. L. Rolston, R. Côté, and M. D. Lukin, Phys. Rev. Lett. **85**, 2208 (2000).

[44] M. Saffman and K. Mølmer, Phys. Rev. Lett. **102**, 240502 (2009).

[45] T. Wilk, A. Gaëtan, C. Evellin, J. Wolters, Y. Miroshnychenko, P. Grangier, and A. Browaeys, Phys. Rev. Lett. **104**, 010502 (2010).

[46] D. D. B. Rao and K. Mølmer, Phys. Rev. Lett. **111**, 033606 (2013).

[47] H. Jo, Y. Song, M. Kim, and J. Ahn, Phys. Rev. Lett. **124**, 033603 (2020).

[48] D. Møller, L. B. Madsen, and K. Mølmer, Phys. Rev. Lett. **100**, 170504 (2008).

[49] M. Saffman, I. I. Beterov, A. Dalal, E. J. Páez, and B. C. Sanders, Phys. Rev. A **101**, 062309 (2020).

[50] X.-F. Shi, Phys. Rev. Appl. **14**, 054058 (2020).

[51] M. Li, F.-Q. Guo, Z. Jin, L.-L. Yan, E.-J. Liang, and S.-L. Su, Phys. Rev. A **103**, 062607 (2021).

[52] S. Ebadi, A. Keesling, M. Cain, T. T. Wang, H. Levine, D. Bluvstein, G. Semeghini, A. Omran, J.-G. Liu, R. Samajdar, X.-Z. Luo, B. Nash, X. Gao, B. Barak, E. Farhi, S. Sachdev, N. Gemelke, L. Zhou, S. Choi, H. Pichler, S.-T. Wang, M. Greiner, V. Vuletić, and M. D. Lukin, Science **376**, 1209 (2022).

[53] T. M. Graham, Y. Song, J. Scott, C. Poole, L. Phuttitarn, K. Jooya, P. Eichler, X. Jiang, A. Marra, B. Grinkemeyer, M. Kwon, M. Ebert, J. Cherek, M. T. Lichtman, M. Gillette, J. Gilbert, D. Bowman, T. Ballance, C. Campbell, E. D. Dahl *et al.*, Nature (London) **604**, 457 (2022).

[54] C. Dlaska, K. Ender, G. B. Mbeng, A. Kruckenhauser, W. Lechner, and R. van Bijnen, Phys. Rev. Lett. **128**, 120503 (2022).

[55] H. Weimer, M. Muller, I. Lesanovsky, P. Zoller, and H. P. Buchler, Nat. Phys. **6**, 382 (2010).

[56] H. Kim, Y. J. Park, K. Kim, H.-S. Sim, and J. Ahn, Phys. Rev. Lett. **120**, 180502 (2018).

[57] T. L. Nguyen, J. M. Raimond, C. Sayrin, R. Cortiñas, T. Cantat-Moltrecht, F. Assemat, I. Dotsenko, S. Gleyzes, S. Haroche, G. Roux, T. Jolicoeur, and M. Brune, Phys. Rev. X **8**, 011032 (2018).

[58] P. Scholl, M. Schuler, H. J. Williams, A. A. Eberharter, D. Barredo, K.-N. Schymik, V. Lienhard, L.-P. Henry, T.-C. Lang, T. Lahaye, A. M. Läuchli, and A. Browaeys, Nature (London) **595**, 233 (2021).

[59] E. Sjöqvist, D.-M. Tong, L. M. Andersson, B. Hessmo, M. Johansson, and K. Singh, New J. Phys. **14**, 103035 (2012).

[60] G.-F. Xu, J. Zhang, D.-M. Tong, E. Sjöqvist, and L. C. Kwek, Phys. Rev. Lett. **109**, 170501 (2012).

[61] B.-J. Liu, X.-K. Song, Z.-Y. Xue, X. Wang, and M.-H. Yung, Phys. Rev. Lett. **123**, 100501 (2019).

[62] P.-Z. Zhao, X. Wu, and D.-M. Tong, Phys. Rev. A **103**, 012205 (2021).

[63] Y. Dong, C. Feng, Y. Zheng, X.-D. Chen, G.-C. Guo, and F.-W. Sun, Phys. Rev. Res. **3**, 043177 (2021).

[64] S. Liu, J.-H. Shen, R.-H. Zheng, Y.-H. Kang, Z.-C. Shi, J. Song, and Y. Xia, Front. Phys. **17**, 21502 (2022).

[65] P. Shen, T. Chen, and Z.-Y. Xue, Phys. Rev. Appl. **16**, 044004 (2021).

[66] E. Herterich and E. Sjöqvist, Phys. Rev. A. **94**, 052310 (2016).

[67] Z. Zhu, T. Chen, X. Yang, J. Bian, Z.-Y. Xue, and X. Peng, Phys. Rev. Appl. **12**, 024024 (2019).

[68] G.-F. Xu, C.-L. Liu, P.-Z. Zhao, and D.-M. Tong, Phys. Rev. A **92**, 052302 (2015).

[69] E. Sjöqvist, Phys. Lett. A **380**, 65 (2016).

[70] P.-Z. Zhao, G.-F. Xu, Q.-M. Ding, E. Sjöqvist, and D. M. Tong, Phys. Rev. A **95**, 062310 (2017).

[71] G.-F. Xu, D.-M. Tong, and E. Sjöqvist, Phys. Rev. A **98**, 052315 (2018).

[72] G. T. Genov, D. Schraft, N. V. Vitanov, and T. Halfmann, Phys. Rev. Lett. **118**, 133202 (2017).

[73] P.-Z. Zhao, X.-D. Cui, G.-F. Xu, E. Sjöqvist, and D.-M. Tong, Phys. Rev. A **96**, 052316 (2017).

[74] B.-J. Liu, S.-L. Su, and M.-H. Yung, Phys. Rev. Res. **2**, 043130 (2020).

[75] L.-N. Sun, L.-L. Yan, S.-L. Su, and Y. Jia, Phys. Rev. Appl. **16**, 064040 (2021).

[76] J. Niu, B.-J. Liu, Y. Zhou, T. Yan, W. Huang, W. Liu, L. Zhang, H. Jia, S. Liu, M.-H. Yung, Y.-Z. Chen, and D.-P. Yu, Phys. Rev. Appl. **17**, 034056 (2022).

[77] K. Singer, J. Stanojevic, M. Weidemüller, and R. Côté, J. Phys. B **38**, S295 (2005).

[78] X. Rong, J.-P. Geng, F.-Z. Shi, Y. Liu, K.-B. Xu, W.-C. Ma, F. Kong, Z. Jiang, Y. Wu, and J.-F. Du, Nat. Commun. **6**, 8748 (2015).

[79] X. Wang, L. S. Bishop, J. P. Kestner, E. Barnes, K. Sun, and S. D. Sarma, Nat. Commun. **3**, 997 (2012).

[80] I. I. Beterov, I. I. Ryabtsev, D. B. Tretyakov, and V. M. Entin, Phys. Rev. A **79**, 052504 (2009).

[81] B. T. Torosov and N. V. Vitanov, arXiv:2206.14283.